# Photoproduction of Neutral Pions at Forward Angles*

KARL BERKELMAN† AND JAMES A. WAGGONER
*Laboratory of Nuclear Studies, Cornell University, Ithaca, New York*
(Received October 12, 1959)

The bremsstrahlung beam of the Cornell Bev electron synchrotron has been used to study the reaction $\gamma+p\rightarrow\pi^0+p$ over the photon energy range 250 Mev to 1 Bev, and for center-of-mass pion angles between 20° and 70°. The recoil protons, of energies between 10 and 60 Mev, were identified and their energies determined using a range telescope of eight thin plastic scintillators enclosed in a vacuum chamber with the thin liquid hydrogen target. Correlated pulse-height information was obtained by photographing an oscilloscope display and was used to sort out the protons from mesons and electrons. Corrections were made for the background of photoprotons from the Mylar target cup, the energy loss of the protons in the liquid hydrogen, absorption and scattering in the counter telescope, and the variation of beam intensity profile with energy. Compared with previous experiments and extrapolations the results show a somewhat smaller forward differential cross section above 400 Mev. The angular distributions obtained from a least-squares fit to all existing data indicate a $d_{\frac{3}{2}}$ assignment for the 760-Mev resonance level. Other implications of the data are also discussed.

## INTRODUCTION

SINCE the discovery of the neutral pion much experimental work has been done on $\pi^0$ photoproduction in hydrogen. A variety of techniques have been used. For energies over 100 Mev above threshold the most successful method has been to observe the energy and angle of the recoil proton. It is clear however, from the kinematics plot (Fig. 1) that this method becomes difficult at forward $\pi^0$ angles. If the pion goes forward, the proton goes backward in the center-of-mass system and consequently has very little energy in the laboratory system. Experiments using conventional counter techniques[1–4] have left large gaps at the forward angles. These gaps have been partially filled by experiments using nuclear emulsions to observe the low-energy protons,[5,6] but the statistics are still rather poor.

In the present experiment an attempt has been made using scintillation counters to identify and measure the energy of recoil protons down to about 10 Mev, and thus to cover the forward angle photoproduction of neutral pions from about 250 to 1000 Mev photon energy. The experiment was motivated by the desire not only to complete the experimental picture of the $\pi^0$ angular distribution but also in particular to get more accurate information on the front-back asymmetry—that is, the $B$ coefficient in the expansion $d\sigma/d\Omega=A+B\cos\theta+C\cos^2\theta$. The asymmetry arises only from the interference of states of opposite parity, and can therefore provide information on the $s$-wave amplitude and the angular momentum assignments for the higher energy resonances.

## EXPERIMENTAL METHOD

The experimental apparatus was designed around four major difficulties involved in counting low-energy protons. First, the stopping power of the target for low-energy protons had to be minimized. This eliminated the carbon-hydrocarbon subtraction method as a possibility and implied a thin liquid hydrogen target with thin walls. Secondly, in order to separate protons from the background of charged mesons and electrons one must require that the lowest energy protons observed must still pass through at least two counters. This meant that the scintillators had to be very thin. Thin

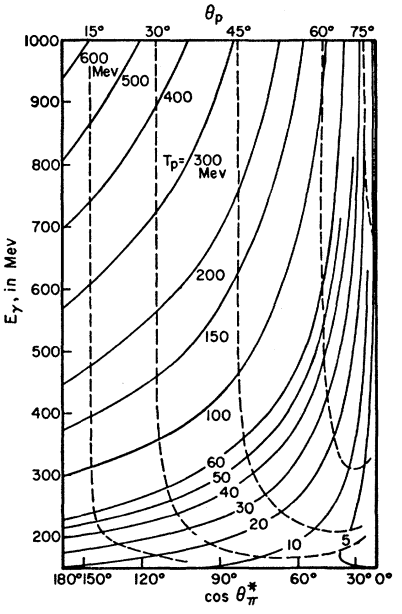


FIG. 1. Kinematics for the reaction $\gamma+p\rightarrow\pi^0+p$. Recoil proton laboratory angle and energy as functions of the photon energy (lab) and the center-of-mass pion angle.

* Supported in part by the joint program of the Office of Naval Research and the U. S. Atomic Energy Commission.
† Corning Glass Works Predoctoral Fellow 1958–1959.
[1] D. C. Oakley and R. L. Walker, Phys. Rev. **97**, 1283 (1955).
[2] J. W. DeWire, H. E. Jackson, and R. M. Littauer, Phys. Rev. **110**, 1208 (1958).
[3] P. C. Stein and K. C. Rogers, Phys. Rev. **110**, 1209 (1958).
[4] J. I. Vette, Phys. Rev. **111**, 622 (1958).
[5] Y. Goldschmidt-Clermont, L. S, Osborne, and M. B. Scott, Phys. Rev. **97**, 188 (1955).
[6] W. S. McDonald, V. Z. Peterson. and D. R. Corson, Phys. Rev. **107**, 577 (1957).

scintillators, however, can give only poor light collection efficiency, therefore poor photoelectron statistics and poor pulse-height resolution. Thirdly, the ratio of low-energy protons from hydrogen and from whatever material contains the liquid hydrogen may well be quite small. Photoprotons in hydrogen come only from $\pi^0$ production, known to be small at forward angles, especially at high photon energies, while in heavier elements photonuclear disintegration gives large numbers of low-energy protons. The ratio gets worse as the target volume is made smaller. Fourthly, the angle and energy aperture of the proton counting system must be small enough to define the photon energy and center-of-mass pion angle sufficiently well for a significant cross-section measurement. A look at the kinematics curves (Fig. 1) shows that as the photon energy increases, its definition by a given $\Delta\theta_p$ and $\Delta T_p$ becomes worse. For a meaningful measurement $\Delta\theta_p$ should be of the order of a degree or two. Of course, the smaller the angle and energy counting aperture, the lower the counting rates.

The liquid hydrogen target used was a modification of one built by F. E. Mills and others. The original design was modeled after the target built by Whalin and Reitz.[7] The hydrogen exposed to the synchrotron beam was contained in a Mylar cup connected to a larger liquid hydrogen reservoir. The cup and reservoir were surrounded by a liquid nitrogen cooled radiation shield with openings for the gamma-ray beam and the proton recoils. The volume around the nitrogen and hydrogen vessels was maintained at high vacuum. The target cup itself was a 1.2-cm diameter $2\frac{3}{4}$-inch long tube of 0.0005-inch Mylar glued to a brass tube at the top and fitted with a small copper cap at the bottom. Facilities were provided for evacuating the target cup separately from the reservoir for background runs.

The proton counters were placed in the same vacuum chamber with the hydrogen target (Fig. 2). The beam windows were made wide enough to enable one to obtain any proton angle relative to the beam from 45° to 85°

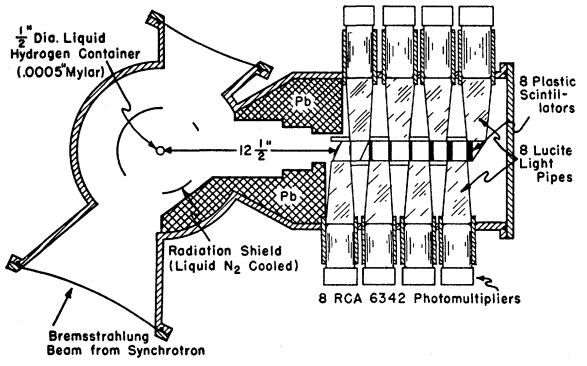


FIG. 2. Plan view of the lower portion of the hydrogen target vacuum chamber, showing the target cup and the proton counter telescope.

[7] E. A. Whalin, Jr., and R. A. Reitz, Rev. Sci. Instr. **26**, 1203 (1955).

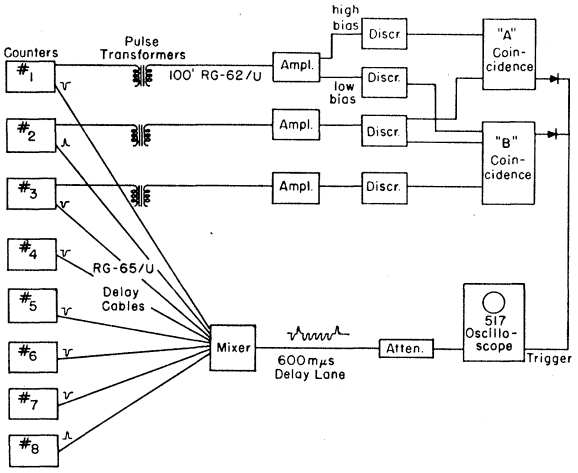


FIG. 3. Block diagram of the detection electronics used in the experiment. Not shown are the high-voltage power supplies and scalers.

simply by rotating the whole chamber about the target cup. One can see from the kinematics curves (Fig. 1) that this angular range is sufficient to cover most of the $\pi^0$ production in the center-of-mass forward hemisphere above 250-Mev photon energy.

Because of the low counting rates expected it was decided to construct a proton counter telescope sensitive to a wide range of energies. Using eight scintillators one can count protons in six range intervals simultaneously by noting coincidences $12\bar{3}$, $123\bar{4}$, etc. (bar denotes anticoincidence). The width of the scintillators was fixed by the necessarily small angular aperture $\Delta\theta_p$, but the height was made several times larger to maximize the counting rate. The counters were made of plastic scintillators in thicknesses such that the first corresponded to the range of a 5-Mev proton, the first and second—10 Mev, the first three—20 Mev, and so on. For example, a proton stopping in the seventh counter must have had an energy between 50 and 60 Mev. Once the thicknesses of the scintillators were determined one could predict from the range-energy tables the energy loss in each counter as a function of the entering proton energy. If one does the same for pions, one notices that for pions and protons stopping in the $n$th counter with the same energy loss, the energy loss of the proton in the $(n-1)$st counter is at least twice that of the pion. Electrons are even more easily distinguished. It was on this basis that the selection of protons from mesons and electrons was made.

The solid angle subtended at the target by the counter telescope was determined by the size of the first scintillator, which was 1.2 cm by 10 cm. The others were made oversize to minimize scattering out. The first counter was about $12\frac{1}{2}$ inches from the target.

Correlated pulse-height information from the eight counters in coincidence was recorded by displaying the pulses on an oscilloscope and photographing the traces.

TABLE I. Experimental data and errors.

| $\theta_p$ | No. of counters | $k$, Mev | $\theta_{\pi^*}$, deg | $d\sigma/d\Omega^*$, $\mu$b/sr | Percent error Counting statistics | Other |
|---|---|---|---|---|---|---|
| 48° | 2 | 228± 17 | 49.7±7 | 3.6±1.3 | 28 | 22 |
| | 3 | 247± 13 | 60.7±6 | 7.7±0.7 | 6 | 6 |
| | 4 | 274± 16 | 67.1±3 | 17.1±0.9 | 3 | 4 |
| | 5 | 307± 18 | 70.8±3 | 23.6±1.0 | 3 | 3 |
| | 6 | 342± 18 | 73.1±2 | 24.4±1.1[a] | 3 | 3 |
| | 7 | 375± 18 | 75.2±2 | 15.8±1.0 | 4 | 5 |
| 52° | 2 | 251± 11 | 44.9±6 | 6.2±1.6 | 18 | 17 |
| | 3 | 272± 14 | 54.4±4 | 11.8±0.6 | 3 | 4 |
| | 4 | 304± 17 | 60.1±3 | 21.4±1.0 | 3 | 4 |
| | 5 | 343± 19 | 63.5±2 | 20.2±0.9 | 3 | 3 |
| | 6 | 382± 20 | 65.5±2 | 14.5±0.8 | 4 | 4 |
| | 7 | 422± 21 | 66.7±2 | 9.7±0.7 | 5 | 5 |
| 56° | 2 | 279± 14 | 40.0±5 | 12.9±2.2 | 7 | 15 |
| | 3 | 305± 16 | 48.5±4 | 17.8±0.9 | 3 | 5 |
| | 4 | 342± 20 | 53.4±3 | 19.0±1.0 | 2 | 5 |
| | 5 | 387± 22 | 56.4±2 | 11.2±0.6 | 3 | 4 |
| | 6 | 435± 24 | 58.0±2 | 7.6±0.5 | 5 | 5 |
| | 7 | 482± 26 | 59.0±2 | 4.1±0.4 | 8 | 5 |
| 60° | 2 | 318± 16 | 36.6±5 | 14.2±2.6 | 6 | 17 |
| | 3 | 351± 20 | 42.5±4 | 14.3±1.2 | 2 | 5 |
| | 4 | 396± 25 | 46.7±3 | 9.8±0.6 | 4 | 5 |
| | 5 | 448± 27 | 49.4±2 | 5.3±0.4 | 5 | 4 |
| | 6 | 508± 30 | 50.6±2 | 2.5±0.3 | 10 | 5 |
| | 7 | 570± 33 | 51.2±2 | 1.9±0.3 | 14 | 6 |
| 63° | 2 | 357± 20 | 32.9±5 | 9.3±2.1 | 10 | 21 |
| | 3 | 395± 25 | 38.3±3 | 9.0±0.7 | 5 | 6 |
| | 4 | 451± 31 | 42.0±2 | 5.8±0.5 | 6 | 5 |
| | 5 | 516± 34 | 44.0±2 | 2.5±0.3 | 11 | 5 |
| | 6 | 587± 39 | 45.3±2 | 1.7±0.3 | 16 | 5 |
| | 7 | 660± 45 | 45.6±2 | 1.0±0.3 | 29 | 7 |
| 66° | 2 | 409± 25 | 29.2±4 | 6.1±1.8 | 15 | 25 |
| | 3 | 457± 30 | 33.9±3 | 5.4±0.6 | 7 | 8 |
| | 4 | 525± 40 | 36.9±2 | 3.0±0.4 | 11 | 6 |
| | 5 | 610± 45 | 38.6±2 | 1.2±0.3 | 23 | 6 |
| | 6 | 703± 55 | 39.1±2 | 1.1±0.3 | 25 | 6 |
| | 7 | 802± 65 | 39.5±2 | 0.9±0.3 | 32 | 8 |
| 68° | 3 | 509± 40 | 30.9±3 | 3.2±0.4 | 8 | 7 |
| | 4 | 592± 55 | 33.7±2 | 1.8±0.3 | 12 | 6 |
| | 5 | 698± 65 | 34.7±2 | 0.9±0.2 | 21 | 6 |
| | 6 | 808± 80 | 35.6±2 | 1.1±0.2 | 17 | 6 |
| | 7 | 927± 95 | 35.8±2 | 1.0±0.2 | 20 | 8 |
| 70° | 2 | 509± 40 | 24.5±3 | 3.1±1.4 | 29 | 38 |
| | 3 | 578± 45 | 28.0±2 | 2.0±0.5 | 18 | 13 |
| | 4 | 685± 60 | 30.3±2 | 1.9±0.4 | 16 | 8 |
| | 5 | 805± 80 | 31.5±2 | 2.0±0.3 | 14 | 7 |
| 72° | 3 | 675± 65 | 24.9±2 | 1.4±0.4 | 24 | 16 |
| | 4 | 800± 90 | 26.9±2 | 1.4±0.3 | 18 | 9 |
| | 5 | 940±100 | 27.6±2 | 1.0±0.3 | 27 | 10 |

[a] Normalization point.

Figure 3 shows a block diagram of the electronics system used to achieve this. Fast pulses from each counter were passed through various lengths of delay cable. The signals were then mixed and fed into the vertical amplifier input of a Tektronix 517 oscilloscope. Each trace then showed in sequence the pulses from all the counters. The oscilloscope sweep was triggered by either one of two coincidence circuits, one designed to respond to all protons stopping in the second counter and the other responding to all protons stopping in any of the succeeding counters.

The layout of equipment along the gamma-ray beam line was as follows: at 2.6 meters from the internal radiating target in the synchrotron,[8] a $\frac{1}{4}$-in.$\times\frac{3}{8}$-in. collimator followed by a permanent $H$ magnet to remove electrons from the beam; at 6.4 meters, a secondary collimator flanked by a one-foot thick wall of lead and followed by a beam hole through a two-foot wall of concrete; at 7.4 meters, the liquid hydrogen target chamber; and at 14.6 meters, a concrete cave enclosing the beam monitor.

Synchrotron runs were made at nine laboratory proton angles (see Table I). For each laboratory angle the maximum bremsstrahlung energy $E$ was chosen such that (1) $E$ was above the photon energy required to make 60-Mev proton recoils from $\gamma+p\rightarrow\pi^0+p$ in the angular interval subtended by the counter telescope, and (2) $E$ was below the energy required to make proton recoils from $\gamma+p\rightarrow\pi^0+\pi^0+p$ at the counter telescope. Each run consisted of around 10 000 "hydrogen in" counts (60 to 90% of which were accepted protons) and enough "hydrogen out" counts to give comparable statistics.

The oscilloscope film data were scanned using a microfilm projector. The scanner recorded the number of pulses and the height of the last two pulses. Anticoincidences (eighth counter) and accidental near-coincidences were rejected. For each number-of-pulses category the two measured pulse heights were plotted as in Fig. 4. From range-energy tables one can predict the locus of energy losses in a pair of counters; this is also shown (for the four-pulse category) in Fig. 4. The two plots do not correspond exactly for several reasons: (1) the light output of the scintillators is not exactly proportional to energy loss; (2) pions occasionally decay so fast that the muon pulse cannot be distinguished from the stopping proton pulse; (3) the nonuniformity of light collection efficiency over the scintillator area and

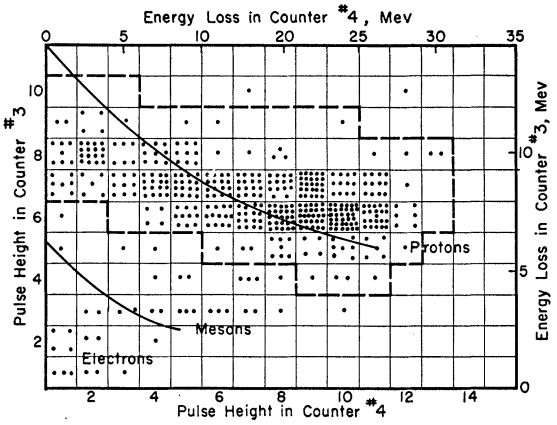


FIG. 4. A typical pulse-height correlation plot obtained from one roll of film data. Each point represents the last two pulse heights of a four-pulse trace. Also shown are the loci of energy losses for protons and charged mesons stopping in the fourth counter. The dashed line encloses the points which were taken to be protons between 20 and 30 Mev.

[8] The Cornell Bev electron synchrotron has been described in an Office of Naval Research Report Nonr-401, 26 (unpublished).

the statistics of photoelectron emission at the photomultiplier cathode cause a spread in pulse heights which can be as much as 20 to 30%. Nevertheless, it is clear from Fig. 4 that one can separate out the pulses which correspond to protons, with an uncertainty of a few percent or less. The separation was quite straightforward for all range intervals except the first (5 to 10 Mev). In that case the resolution was poorer and the electron background was much higher. There the uncertainty in the number of protons was 14% to 26%.

## DATA REDUCTION

The proton rates obtained for hydrogen in and out, had to undergo several corrections before they were used for the cross section computations.

### A. Target Thickness Correction

The stopping power of the liquid hydrogen for low-energy protons had two effects. First, the proton energy as measured by the range telescope was not exactly the energy at which the proton was produced in the target. This meant, for example, that in the second range interval (first three counters in coincidence), which nominally corresponded to the 10- to 20-Mev interval, were counted some protons between 10 and 17 Mev, all protons between 17 and 20 Mev and some protons between 20 and 24 Mev. Figure 5(a) shows this effective energy resolution function for each range interval. Secondly, when the target cup was filled with liquid hydrogen, the background protons produced in the far side (away from the counter telescope) of the Mylar target wall were slowed down in passing through the target, while during empty-target background runs protons from the far-side Mylar target wall passed through only a negligible thickness of Mylar. The corresponding effective energy resolution functions are shown in Figs. 5(b) and (c). The fraction of the empty-target proton energy spectrum which corresponded to protons from the far-side Mylar was integrated using the weighting functions in Fig. 5(c) to obtain the actual far-side contribution to the full-target rates. The resulting total true background rates were then subtracted from the full-target rates to get the net hydrogen rates. The correction was appreciable only for the first two range intervals; for proton energies above 20 Mev the stopping power of the hydrogen was insignificant. For the 5- to 10-Mev proton interval the correction was sometimes comparable to the total net rate.

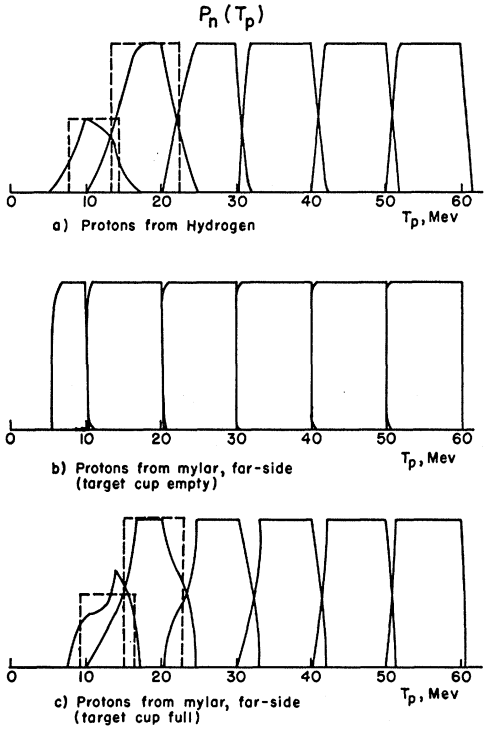


FIG. 5. The actual energy resolution functions for the various counter telescope range intervals, taking into account energy loss in the target. $P_n(T_p)$ is the probability for a photoproton produced with energy $T_p$ of stopping in the $n$th counter. The dashed lines show the equal-area approximations used in the calculations.

### B. Absorption and Scattering in the Counters

The data were corrected for absorption and scattering in the counter telescope. This amounted to about 6% for the 50 to 60-Mev interval and progressively less for the others.

### C. Beam Profile

In order to maximize the counting rate while minimizing the sensitivity to target alignment, the beam was collimated to a width somewhat greater than the hydrogen cup diameter. This meant that not all of the photons recorded by the beam monitor passed through the target; and since the target had a circular cross section, not all photons passed through the same thickness of hydrogen. This was further complicated by the fact that the intensity was not uniform over the width of the beam and changed with the peak bremsstrahlung energy. The beam profile, or intensity distribution across its width (integrated along the vertical direction) was measured in a separate experiment.[9] The quantity of interest is

$$K=\frac{\int_{-w}^{w} I(\theta)d\theta}{\int_{-a}^{a}(a^2-\theta^2)^{\frac{1}{2}}I(\theta)d\theta},$$

which is the ratio of the amount of beam recorded by the monitor ($w$ is the angular width of the collimator) to the amount of beam passing through the target (angular width $a$), weighted by its path length in the target. $K$

[9] The authors are indebted to E. Malamud and D. N. Olson for their help in this measurement.

was computed for each run. It was assumed that the beam profile distribution $I(\theta)$ depended on the end-point energy $E$ in such a way that $I(\theta E)$ was independent of $E$. This implies, for example that the rms angle varies as $E^{-1}$ as one would expect assuming the spreading is due to the multiple scattering of the electrons in the synchrotron target before they radiate.

The counting rate per unit beam is given in terms of the cross section by

$$R=(\text{nuclei/cm}^2)(d\sigma/d\Omega^*)\Delta\Omega^* n(k,\Delta k)(\langle w\rangle_{\text{target}}/\langle w\rangle_{\text{beam}}).$$

$n(k,\Delta k)$ is the number of photons per unit beam in the interval $\Delta k$ around energy $k$; $\langle w\rangle_{\text{target}}/\langle w\rangle_{\text{beam}}$ takes into account the fact that the beam is wider than the target; and asterisks denote center-of-mass coordinates. Substituting $(\text{nuclei/cm}^2)=\rho N_{\text{Avog}}A^{-1}\langle t\rangle_{\text{target}}$, $n(k,\Delta k)=QF(k,E)\Delta k/k$, $\Delta\Omega^*=\Delta\cos\theta_\pi^*\Delta\phi_p$, and $\langle t\rangle_{\text{target}}\langle w\rangle_{\text{target}}/\langle w\rangle_{\text{beam}}=K^{-1}$, this becomes

$$R=\rho N_{\text{Avog}}A^{-1}(d\sigma/d\Omega^*)\Delta\phi_p\bar{k}^{-1}\left(\int d\cos\theta_\pi^* dk\right)\times F(\bar{k},E)Q2dK^{-1}.$$

Here $\rho$ is the liquid hydrogen density, $F(\bar{k},E)$ is the bremsstrahlung spectrum function ($\int kF(k,E)dk=1$), $Q$ is the number of equivalent quanta per unit beam, and $d$ is the radiator to target distance in meters. Solving for the cross section,

$$\frac{d\sigma}{d\Omega^*}=\left(\frac{A}{\rho N_{\text{Avog}}2d\Delta\phi_p}\right)\frac{RK}{CQ}.$$

In the brackets are grouped all the factors which were constant throughout the experiment. $R$ is the counting rate per unit beam for a particular proton interval at a particular lab angle, corrected for background and for absorption and scattering. $K$ is the beam profile correction factor described above.

$Q$ is the number of equivalent quanta per "sweep," the unit of beam used at Cornell (one sweep is approximately $5\times10^{12}$ Mev of integrated gamma-ray energy), and is given by $E^{-1}\times(\text{Mev/coulomb})\times(\text{coulombs/sweep})$. For some of the earlier runs it was convenient to use the old one-inch copper ionization chamber. Its sensitivity (Mev/coulomb) is energy dependent. For the later runs a Quantameter was used. Its calibration is constant and has been computed from shower theory: $4.80\times10^{18}$ Mev/coulomb.[10] The two chambers have been intercalibrated at a number of energies, and an absolute pair-spectrometer calibration of the old chamber has been made at two energies.[11] All Cornell and Cal Tech calibrations are now accurate and consistent to better than 3%.[12] Besides the Mev/coulomb for the ion chamber, $Q$ also involves the coulombs/sweep for the charge integrating circuit.[13] This has been calibrated with a standard charge source and gives 1.002 microcoulombs per sweep. The energy $E$ of the circulating electrons in the synchrotron is measured by integrating the magnet voltage from injection time to the time at which the beam is brought out. This instrument has been calibrated by direct measurement of the magnetic field in the synchrotron and by observing the maximum electron pair energy in a pair spectrometer.[11] The uncertainty in $E$ is probably less than 1% below 1 Bev, but increases to 2 or 3% at the highest energies because of magnet saturation effects.

$C$ is the "kinematic factor":

$$C=\left(\int d\cos\theta_\pi^* dk\right)\bar{k}^{-1}F(\bar{k},E),$$

where the integral is taken over the "rectangle" in $k\times\cos\theta_\pi^*$-space cut out by the lab proton energy and angle intervals $\Delta T_p$ and $\Delta\theta_p$. Actually the intervals are more accurately described in terms of weighting functions: the energy weighting functions are shown in Fig. 5(a); the angular resolution function was triangular, 2.2° wide at half maximum. For convenience in computation, however, the weighting functions were approximated by rectangular functions of the same area, giving simple intervals $\Delta T_p$ and $\Delta\theta_p$. For $F(\bar{k},E)$ the best-fit "thick target spectrum" indicated by the pair spectrometer data[11] (corresponding to 0.08 radiation lengths) was used.

The constant factor in brackets in the above expression for the cross section contains only one parameter which is not precisely determined or easily measured: the liquid hydrogen density $\rho$ in the target cup. This is likely to deviate considerably from the handbook value (0.070 g/cm³), since the hydrogen was continually boiling. To avoid this uncertainty in the data the quantity in brackets was "measured" by normalizing all measured cross sections to the best-fit previous value at one point. The normalized point was at $k\approx342$ Mev, $\theta_\pi^*\approx73°$. This particular point was chosen because (1) the cross section is high and the statistics good, (2) the proton identification uncertainty is negligible, (3) the target thickness and background corrections are small, and (4) the previous data[6] are probably reliable.

## ERRORS

### A. Statistical

Although about the same total number of full-target counts were taken at each laboratory angle, the statistical accuracy of the data for the various proton range intervals varied widely, depending on the cross section and the amount of empty-target background subtracted (see Table I).

[10] R. R. Wilson, Nuclear Instr. **1**, 101 (1957).
[11] E. Malamud (unpublished).
[12] J. W. DeWire (unpublished).
[13] R. M. Littauer, Rev. Sci. Instr. **25**, 148 (1954).

### B. Proton Identification

The uncertainty in each case was estimated by drawing reasonable upper and lower limits on the proton band (Fig. 4) and noting the difference.

### C. Corrections

The target thickness correction described above cannot be made very precise. It is estimated to give an uncertainty of 4% in the corrected background rate for the 5- to 10-Mev interval and progressively less for the others. It is most significant in the cases where the background is a large fraction of the total counts.

The uncertainty in the absorption and scattering loss in the counters was estimated to be 20% of the correction.

The uncertainty in the beam profile correction factor $K$ is due primarily to the uncertainty in the measured beam profile and in the radius $a$ of the hydrogen target. This, however, is largely absorbed in the normalization.

### D. Kinematic factor $C$

Uncertainty in the determination of $C$ arose from the approximations used in evaluating the integral (typically about 2%) and from the uncertainty in the photon spectrum function $F(k,E)$. The latter error was set equal to the difference between the Bethe-Heitler thin-target spectrum[14] and the thick-target spectrum which best fits the pair spectrometer data.[11]

### E. Monitor

The errors listed in Table I are errors in the relative cross sections. Any absolute error in monitor calibration is absorbed in the normalization. One source of variable error which was not realized at first is the fact that the old ion chamber is subject to recombination loss at high beam intensities. Using Malamud's measurements[15] of this effect, we have made corrections to the early data from zero to 4%. The uncertainty was estimated to be equal to the magnitude of the correction.

### F. Scanning

A re-scan of about 30% of the data showed about 2% scanning errors.

### G. Discriminator Biases

The discriminator biases for the coincidence circuits which trigger the oscilloscope were set low enough to allow all protons between 5 and 60 Mev to be counted and high enough to keep the electron background reasonable. After some of the early runs had already been made, it was discovered that the pulse-height sensitivity of the first scintillator was lowered when the target was filled with liquid hydrogen. The biases had been set before transferring hydrogen, and consequently afterward the lower tail of the proton pulse-height distribution was missed. After this effect was discovered rough measurements gave an error estimate of 2 to 4% in the early proton rates for the 50- to 60-Mev channel. Rates for proton energies below 50 Mev were only negligibly affected In the later runs the biases were set only after thermal equilibrium had been reached.

### H. Normalization

The uncertainty in the normalization factor is given by the relative error in the experimental data (Table I) at the normalization point, 4.4%, and the error in the previous data, 2.8%. The net uncertainty of 5.2% is common to all the measured cross sections. It is *not* included in the relative errors listed in Table I.

### I. Other Processes

Besides the reaction investigated, there are two others which give photoprotons from hydrogen: the proton Compton effect and multiple meson production. At each laboratory angle the maximum photon energy was chosen so that proton recoils from multiple meson production were kinematically forbidden. This cannot be done in the Compton scattering case, since the available center-of-mass kinetic energy is greater. The data of this experiment then include a small contamination—a few percent at the most[16,17]—from the proton Compton effect. Since the available Compton data are rather sparse no correction was made.

### J. Spread in $k$ and $\theta_\pi^*$

Each cross section, although it is quoted for a particular value of $k$ and $\theta_\pi^*$, is actually a weighted average over the range of $k$ and $\theta_\pi^*$ which is subtended by the lab proton energy interval $\Delta T_p$ and angular aperture $\Delta\theta_p$. There is an additional contribution to $\Delta\theta_p$ from the multiple scattering of the protons as they leave the target. The $\Delta k$ and $\Delta\theta_\pi^*$ limits given in Table I correspond approximately to the points where the weighting is down to half maximum. $\Delta\theta_\pi^*$ is always small—of the order of a few degrees. However, as $k$ increases, $\Delta k$ becomes very large. Beyond about 800 Mev $\Delta k$ becomes comparable to the characteristic energy width of a resonance level.

## RESULTS

The computed $\pi^0$ photoproduction cross sections with their percentage errors are shown in Table I. In order to interpret these data in terms of angular momentum states of the pion-nucleon system, it is convenient to be

[14] W. Heitler, *The Quantum Theory of Radiation* (Oxford University Press, New York, 1954), third edition, p. 242.
[15] E. Malamud (private communication).
[16] T. Yamagata, Ph.D. thesis, University of Illinois, 1956 (unpublished).
[17] R. M. Littauer, J. W. DeWire, and M. Feldman, Bull. Am. Phys. Soc. 4, 253 (1959).

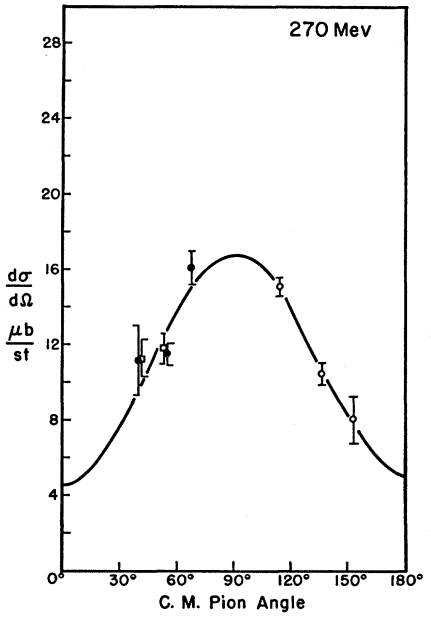


FIG. 6. $\pi^0$ photoproduction angular distribution at 270-Mev lab photon energy. Open circles indicates data of reference 1, squares reference 6, and black circles this experiment. The curve is drawn from the least-squares fit to $A+B\cos\theta+C\cos^2\theta$.

able to plot the angular distribution in the center of mass for a number of values of the photon energy. To complete the picture at larger pion angles data from other $\pi^0$ production experiments[1–4,6] must be included. The most recent and extensive of these experiments have given angular distributions at photon energies around 270, 295, 320, 360, 400, 450, 500, 590, 700, 800, and 950 Mev.

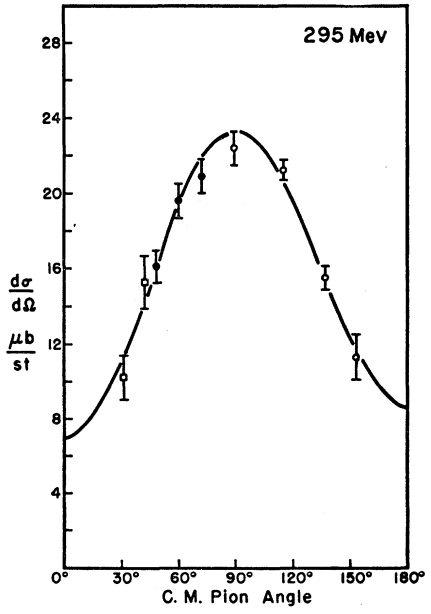


FIG. 7. Angular distribution at 295 Mev. Curve is quadratic least-squares fit.

In the present experiment, however, the center-of-mass angle and photon energy could not be selected entirely at will. Only the lab angle $\theta_p$ could be varied; the proton energies $T_p$ were fixed. It was possible, though, to chose $\theta_p$ values such that most of the data points tended to group within 5% of the selected energies. The few data points with energies more than 5% off were not used in the analysis.

It is still possible for a 5% energy discrepancy to falsify the angular distributions especially near the first resonance where the cross section is very strongly energy dependent. To minimize this effect each cross-section value at the experimental energy was replaced by a value corresponding to the "standard" energy by interpolating at a fixed angle or by scaling according to the energy dependence of the total cross section.

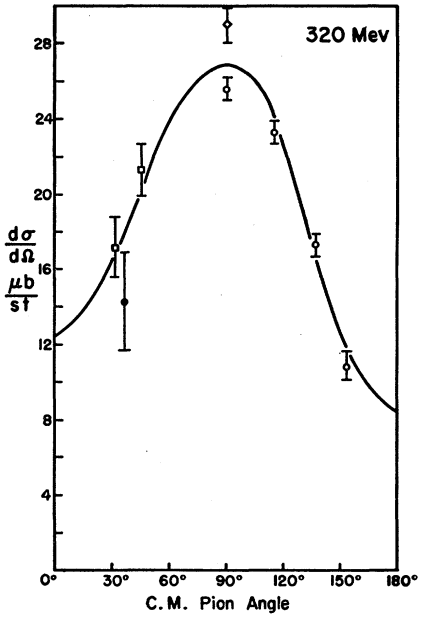


FIG. 8. Angular distribution at 320 Mev. Diamond-shaped point is from the data of reference 2. Curve is quadratic least-squares fit.

In Figs. 6 through 13 are plotted all the recent data on $\pi^0$ photoproduction at the selected photon energies. At the lower energies the present data are in fair agreement with the Cal Tech emulsion data[6] although somewhat lower at 400 and 450 Mev where the corrections in the emulsion experiment are largest. The present experimental results join on quite well with those of the Cal Tech magnet experiment.[1] At higher energies the present data are considerably lower than the Cal Tech values.[4] At each energy there are several points from the present experiment closely spaced in center-of-mass angle, but coming from different runs at different values of $T_p$ and $\theta_p$. It is perhaps conceivable that the systematic errors could be much larger than estimated for some of the points, but it is difficult to

imagine a systematic error which would lower all the points taken under such varied experimental conditions.

A least-squares fit to the first few terms of a power series in $\cos\theta$ was made at each of the selected photon energies. All of the data in Figs. 6 through 13 were included. A three-parameter fit $(A+B\cos\theta+C\cos^2\theta)$ was made at each energy; four- and five-parameter fits were also made at 450 Mev and above. The least-squares coefficients $A$, $B$, $C$, $D$, and $E$ with their computed standard deviations are shown in Table II. The error limits are reliable only if the errors in the data are random, independent, normally distributed, and correctly estimated, and if the true angular distribution can be given accurately by the first few terms of a power series in $\cos\theta$. Since each of these conditions is violated to some degree, the statistically computed standard

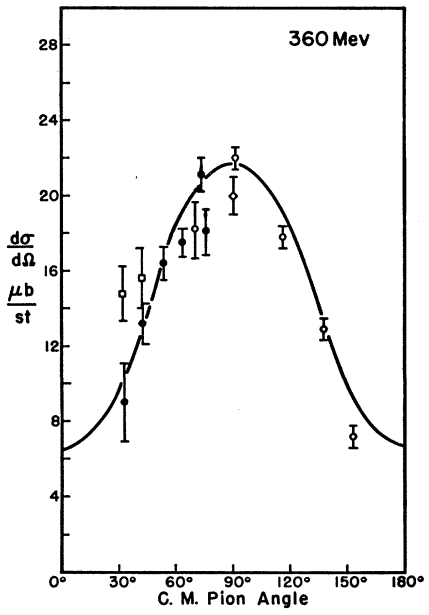


FIG. 9. Angular distribution at 360 Mev. Curve is quadratic least-squares fit.

errors in the coefficients $A$, $B$, $C$, $D$, $E$ are almost certainly too small.

The "adopted" coefficients (Fig. 14, 15) were chosen as follows. Up to and including 400 Mev the three-parameter fit was assumed to be sufficient. The data at 450, 500, and 590 Mev are not consistent and accurate enough to make a reliable determination of the $\cos^3\theta$ and $\cos^4\theta$ contributions. Consequently, the quadratic fit has been adopted as the most reasonable representation of the data in this region. It should be emphasized, however, that this should not be taken as evidence of the absence of the higher powers of $\cos\theta$. From 700 to 950 Mev the best fit was chosen on the basis of the $\chi^2$ goodness of fit test. At 800 Mev this turned out to be the five-parameter fit, but at 700 and 950 Mev the $\chi^2$ probabilities of the three, four, and five-parameter fits

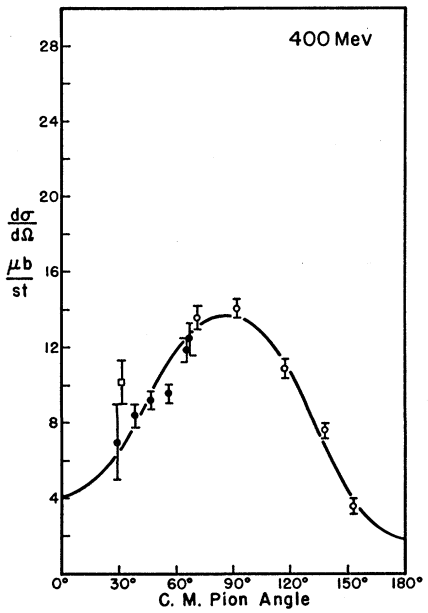


FIG. 10. Angular distribution at 400 Mev. Curve is quadratic least-squares fit.

were all so close that a weighted mean was taken for the adopted coefficients. The total cross section (Fig. 16) is obtained by integrating the least-squares fits: $\sigma=4\pi[A+(B/3)+(C/5)]$.

Comparing the best-fit coefficients with those of earlier experiments, there are several significant differ-

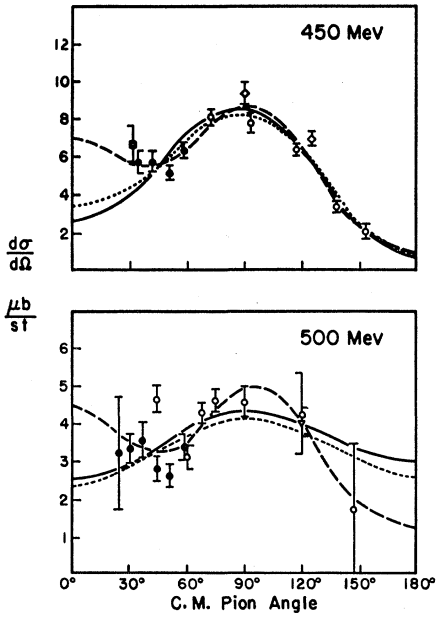


FIG. 11. Angular distributions at 450 and 500 Mev. At 500 Mev the open circles indicate data of reference 4, the triangles reference 3. The solid curve is the quadratic least-squares fit; the dashed curve is the least squares fit to $A+B\cos\theta+C\cos^2\theta+D\cos^3\theta+E\cos^4\theta$; the dotted curve is the "retardation fit" (explained in text).

TABLE II. Least squares analysis: $d\sigma/d\Omega = A + B\cos\theta + C\cos^2\theta + D\cos^3\theta + E\cos^4\theta$.

| $k$, Mev | $A$, μb/sr | $B$ | $C$ | $D$ | $E$ | $\sigma$, μb | Note[a] |
|---|---|---|---|---|---|---|---|
| 270 | 16.8 ±0.6 | −0.3 ±0.5 | −12.0±1.5 | | | 161 ±3 | 1 |
| 295 | 23.3 ±0.5 | −0.8 ±0.5 | −15.6±1.2 | | | 244 ±3 | 1 |
| 320 | 26.9 ±0.4 | 2.0 ±0.7 | −16.4±1.0 | | | 287 ±3 | 1 |
| 360 | 21.8 ±0.4 | −1.4 ±0.4 | −15.2±0.9 | | | 226 ±2 | 1 |
| 400 | 13.7 ±0.3 | 1.1 ±0.3 | −10.8±0.7 | | | 138 ±2 | 1 |
| 450 | 8.3 ±0.2 | 1.0 ±0.2 | −6.6±0.5 | | | 84 ±2 | 1 |
| | 8.2 ±0.2 | −0.5 ±0.6 | −6.2±0.5 | 2.9±1.1 | | | 3 |
| | 8.7 ±0.3 | −1.0 ±0.6 | −10.5±1.9 | 4.0±1.2 | 5.7±2.4 | 80 ±2 | |
| | 8.3 ±0.2 | 1.3 ±0.3 | −6.2±0.5 | | | 83 ±2 | 2 |
| 500 | 4.3 ±0.2 | −0.2 ±0.3 | −1.5±0.6 | | | 49 ±2 | 1 |
| | 4.8 ±0.3 | −1.6 ±0.6 | −4.0±1.1 | 4.6±1.7 | | | 3 |
| | 4.9 ±0.3 | −1.1 ±0.7 | −5.6±1.7 | 2.7±2.3 | 3.5±3.0 | 48 ±4 | |
| | 4.1 ±0.2 | −0.1 ±0.5 | −1.7±0.5 | | | 46 ±2 | 2 |
| 590 | 3.26±0.12 | −0.44±0.21 | −1.8±0.4 | | | 33.2±1.0 | 1 |
| | 3.61±0.15 | −2.02±0.42 | −3.2±0.5 | 3.8±0.9 | | | 3 |
| | 3.45±0.17 | −2.37±0.45 | −1.0±1.2 | 4.6±1.0 | −3.4±1.7 | | 3 |
| 700 | 3.65±0.16 | −0.54±0.18 | −2.7±0.4 | | | 34.7±1.1 | |
| | 3.66±0.16 | −1.06±0.08 | −2.9±0.4 | 1.0±0.8 | | 33.9±1.3 | |
| | 3.88±0.22 | −0.96±0.45 | −5.0±1.4 | 0.6±0.9 | 2.7±1.9 | 34.7±1.5 | |
| | 3.77±0.19 | −0.88±0.29 | −3.9±0.9 | 0.6±0.9 | 1.4±1.9 | 34.5±1.4 | 1, 4 |
| 800 | 3.40±0.08 | −0.68±0.13 | −2.0±0.3 | | | 34.4±0.7 | |
| | 3.59±0.09 | −1.46±0.24 | −2.8±0.3 | 2.0±0.5 | | 33.3±0.9 | |
| | 3.67±0.12 | −1.31±0.27 | −3.7±0.8 | 1.7±0.6 | 1.4±1.2 | 34.0±1.1 | 1 |
| 950 | 1.81±0.07 | −0.89±0.10 | 0.5±0.2 | | | 24.9±0.5 | |
| | 1.71±0.08 | −0.46±0.21 | 0.9±0.3 | −1.2±0.5 | | 25.1±0.7 | |
| | 1.63±0.09 | −0.66±0.24 | 1.9±0.6 | −0.6±0.6 | −1.9±1.0 | 23.9±1.0 | |
| | 1.66±0.09 | −0.59±0.23 | 1.6±0.5 | −0.8±0.6 | −1.2±1.0 | 24.2±0.9 | 1, 4 |

[a] The significance of the numbers is as follows. 1: Adopted fit. 2: Fit to $d\sigma/d\Omega = A + B\cos\theta[1 - \frac{1}{2}\beta^2\sin^2\theta(1 - \beta\cos\theta)^{-1}] + C\cos^2\theta$. 3: $d\sigma/d\Omega < 0$ at some angles. 4: The average of the 3-, 4-, and 5-parameter fits, weighted according to $\chi^2$ probability.

ences to be noted. (1) In the region of the first resonance $B$ is smaller than reported by McDonald, Peterson, and Corson.[6] (2) The 700- and 800-Mev measurements of $D$ and $E$ are smaller than those of Vette,[4] but still of the same sign. (3) At 950 Mev $D$ is negative, instead of positive as reported by Vette. It should be pointed out that at 950 Mev the angular distribution coefficients seem to be varying considerably over an energy range smaller than the experimental energy resolution width. For example, in the present experiment the total resolu-

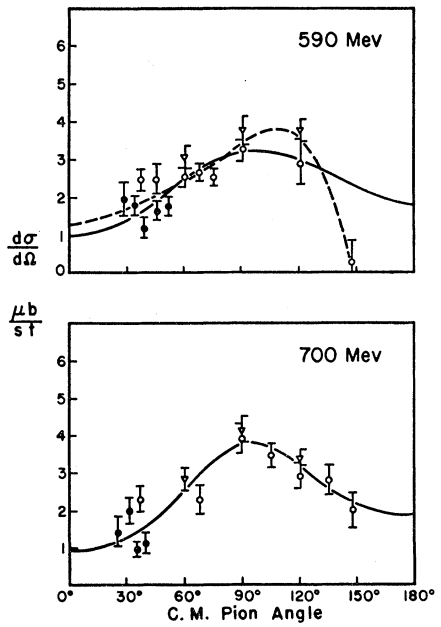


FIG. 12. Angular distributions at 590 and 700 Mev. At 590 Mev the solid curve is the quadratic least-squares fit, the dashed curve the quartic fit. At 700 Mev the curve is an average of the three, four, and five-parameter fits, weighted according to $\chi^2$ probability.

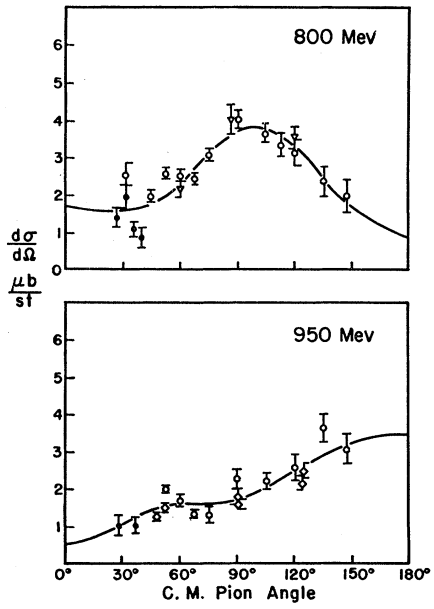


FIG. 13. Angular distributions at 800 and 950 Mev. The 800-Mev curve is the quartic least-squares fit. The 950-Mev curve is an average of the four- and five-parameter fits, weighted according to $\chi^2$ probability.

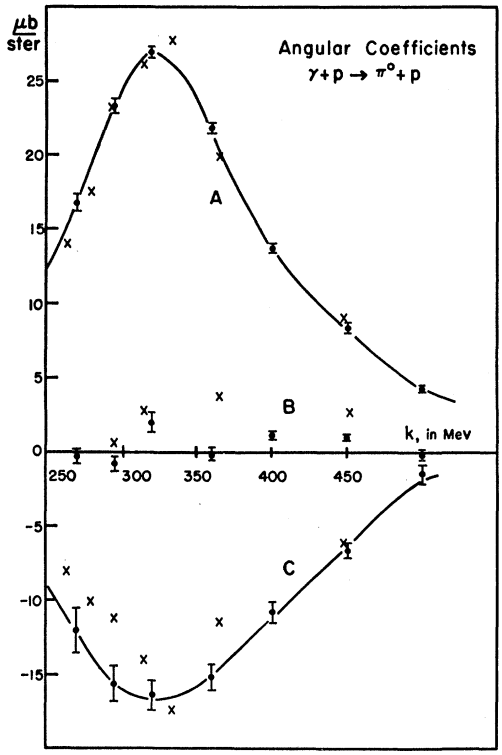


FIG. 14. Angular coefficients obtained from least-squares fit to $d\sigma/d\Omega = A + B\cos\theta + C\cos^2\theta$ from 270 Mev to 500 Mev. The crosses show the dispersion theory predictions of references 19 and 20.

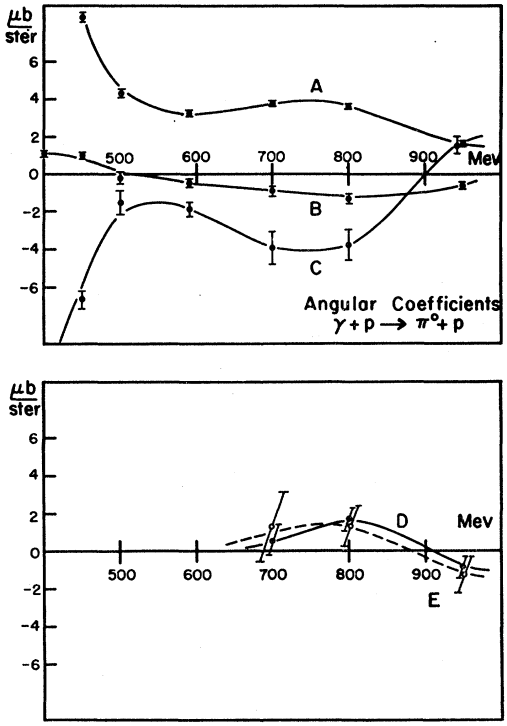


FIG. 15. Angular coefficients obtained from the least-squares fits from 500 to 950 Mev.

tion width at half maximum is around 200 Mev for the 950-Mev points (Table I); in Vette's experiment it varies from about 125 Mev at large angles to about 360 Mev at small angles[18]; in the experiments of DeWire et al.[2] the width is 100 Mev. Until the 950-Mev data are confirmed by an experiment of better energy resolution, the present data must be considered as only tentative.

## INTERPRETATION

Chew, Goldberger, Low, and Nambu[19] have used the dispersion theory approach to derive the photoproduction amplitudes in terms of the scattering phase shifts. This calculation takes into account all nucleon recoil effects to first order in $v/c$ and all $s$ and $p$ waves. It is claimed that the final amplitude should be accurate to 5 or 10% below the first resonance, but should deteriorate rapidly above the resonance. Using these amplitudes and the most recent reliable scattering phase shift determinations, Höhler and Müllensiefen[20] have computed predictions for the angular coefficients $A$, $B$, and $C$ in $\pi^0$ production. In Fig. 14 the crosses show their computed coefficients.

There is some uncertainty in these dispersion theory results arising from experimental error in the scattering phase shifts (especially the small $p$-phases), the uncertainty in the contribution of the electric dipole term $N^+$ of Chew et al., and the approximations used in the derivation. Agreement on the $A$ coefficient is well within theoretical and experimental uncertainties. With respect to the $B$ and $C$ coefficients, both theory and experiment are subject to fairly large uncertainties, so that it is not clear just how significant the disagreement is.

At 450 and 500 Mev the retardation effect, which comes into the direct photoelectric production via the proton recoil current[21,22] should be most prominent, if it is observable at all, since the 33 resonance contribution is decreasing, $v/c$ is increasing, and the effect of higher resonances is probably small. A least squares fit to a cross section of the form

$$d\sigma/d\Omega = A + B\cos\theta[1-\tfrac{1}{2}\beta^2\sin^2\theta(1-\beta\cos\theta)^{-1}] + C\cos^2\theta$$

was made at 450 and 500 Mev. The results are shown in Fig. 11 (dotted curves) and Table II. At both energies the retardation fit deviates only slightly from the simple three-parameter fit. The goodness-of-fit test favors somewhat the retardation effect at 450 Mev, but

[18] J. I. Vette, Ph.D. thesis, California Institute of Technology, 1958 (unpublished), p. 8.
[19] G. F. Chew, M. L. Goldberger, F. E. Low, and Y. Nambu, Phys. Rev. **106**, 1337 (1957).
[20] G. Höhler and A. Müllensiefen, Z. Physik **157**, 30 (1959). We are indebted to these authors for a preprint of their recent work.
[21] G. Bernardini, Suppl. Nuovo cimento **2**, 114 (1955).
[22] B. T. Feld, Ann. Phys. **4**, 189 (1958).

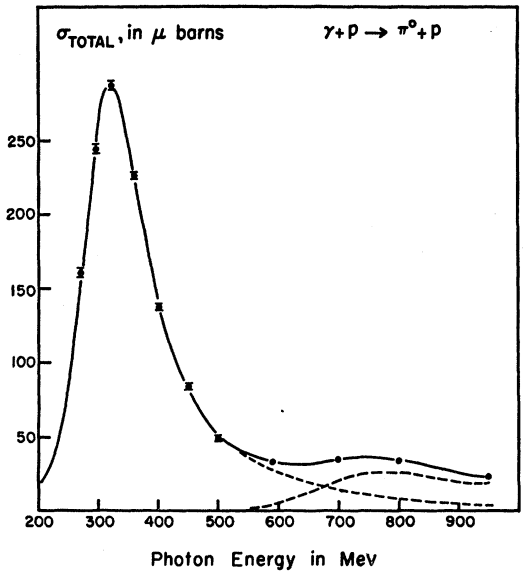


FIG. 16. Total cross section for $\pi^0$ photoproduction, obtained by integrating the least-squares fit angular distributions. The dashed curve is the extrapolation of the 33 resonance contribution and the remainder. The extrapolation is made according to Vette's one-level resonance formula fit.[4] This is consistent with a dispersion theory extrapolation made by Wetherell.[27]

at 500 Mev the no-retardation fit is slightly favored. The evidence for the retardation effect in $\pi^0$ production is therefore inconclusive.

The effect of an electric quadrupole contribution to the predominantly magnetic dipole 33 resonance cross section is seen most directly in the ratio of the $\cos^2\theta$ and isotropic terms in the angular distribution. Neglecting the $s$ wave and small $p$ waves the ratio should be

$$C/A=(-3-6\rho+\rho^2)/(5+2\rho+\rho^2),$$

where $\rho=\sqrt{3}e_2/M_1$ ($e_2$ and $M_1$ are the electric quadrupole and magnetic dipole amplitudes for $J=\frac{3}{2}$). The experimental values for $C/A$ between 270 Mev and 450 Mev are all between $-0.6$ and $-0.8$ with an average value of $-0.69\pm0.02$. This is consistent with pure magnetic dipole excitation of the 33 resonance ($\rho=0$), since the effect of including the $s$-wave is an increase in $|C/A|$ of the same order.

Above 500-Mev photon energy the approximations and simplifications used in the dispersion relation approach are no longer valid. Also the no-recoil, one-meson state, and cutoff approximations of the Chew-Low static theory are unrealistic at the higher energies. Even the phenomenological treatment in terms of a few angular momentum states becomes much more difficult, since many more states can contribute, and Watson's theorem relating the photoproduction phase to the scattering phase shift no longer holds exactly.

The fact that scattering and photoproduction cross sections both show a peak in the $T=\frac{1}{2}$ cross section around 750-Mev photon energy suggests that one angular momentum state may be going through a resonance. The most recent $\pi^-p$ scattering results[23] place the peak at $735\pm25$ Mev/$c$ pion momentum, which gives the same center-of-mass energy as pion production by $740\pm25$ Mev photons. This is consistent with the $\pi^0$ photoproduction data obtained in this and other experiments (Fig. 16). The $\pi^0$ photoproduction angular distribution in the region of the peak—roughly symmetric about a maximum at 90° (Figs. 12, 13)—indicates a dipole photon excitation of a $J=\frac{3}{2}$ state, if we assume that one angular momentum state is dominant. This angular distribution, $5-3\cos^2\theta$, however, is characteristic of both possible parity states: magnetic dipole leading to $p_{\frac{3}{2}}$ and electric dipole leading to $d_{\frac{3}{2}}$. The most reasonable and direct interpretation of the large polarization of the recoil proton observed at 700 Mev[24,25] is that it arises from the interference of the first and second resonances, which must then be of opposite parity. The pion scattering angular distribution[26] also supports this assignment.

Further evidence for the $d$ wave can be obtained from the present $\pi^0$-production data. If the second level has even parity the interference with the first resonance must be symmetric about 90°; any asymmetric term must come from the interference with the $s$ wave. One would expect the asymmetry to change sign somewhere in the region of the second resonance where the phase of the second resonance becomes large and the cosine of the phase difference changes sign. On the other hand, if the second level is odd, the asymmetry arises from the interference with the tail of the first resonance and does not have to change sign. Figure 15 shows that the $B$ coefficient, or asymmetry parameter, remains negative throughout the region of the second resonance, thereby supporting the odd-parity $d$-wave assignment. In fact if we assume that the first and second resonances contribute equally at 700 Mev (see Fig. 16), the polarization

$$P(90°)=\frac{8}{5}\frac{a_p a_d}{a_p^2+a_d^2}\sin(\delta_p-\delta_d), \quad a_p=a_d$$

indicates a phase difference of $\delta_p-\delta_d=48\pm6°$, while the asymmetry coefficient

$$\frac{B}{A}=\frac{4}{5}\frac{a_p a_d}{a_p^2+a_d^2}\cos(\delta_p-\delta_d), \quad a_p=a_d$$

indicates a phase difference of $\delta_p-\delta_d=54\pm15°$.

Because of the very wide energy resolution of the data at 950 Mev and the rapid variation in the angular

[23] J. C. Brisson, J. Detouf, P. Falk-Vairant, L. van Rossum, G. Valladas, and L. C. L. Yuan, Phys. Rev. Letters **3**, 561 (1959).
[24] P. C. Stein, Phys. Rev. Letters **2**, 473 (1959).
[25] J. J. Sakurai, Phys. Rev. Letters **1**, 258 (1958).
[26] R. R. Crittenden, J. H. Scandrett, W. D. Shephard, W. D. Walker, and J. Ballam, Phys. Rev. Letters **2**, 121 (1959); see also Bull. Am. Phys. Soc. 4, 23 (1959); and Proceedings of the 1959 High-Energy Physics Conference at Kiev (unpublished).
[27] A. M. Wetherell, Phys. Rev. **115**, 1722 (1959).

distribution, one cannot expect to draw quantitative conclusions about the third resonance, corresponding to the pion scattering peak observed at 1-Bev lab pion energy.

ACKNOWLEDGMENTS

The authors wish to thank Professor Dale R. Corson for suggesting this investigation and for his help and encouragement during the progress of the experiment. We are also indebted to Dr. Ronald F. Peierls for several stimulating discussions on the theoretical aspects of the problem. Special thanks are due Miss Carol Welker and Miss Elena Citkowitz for their excellent work in reading the film data. Finally, the cooperation of the other members of the synchrotron crew is gratefully acknowledged.

PHYSICAL REVIEW VOLUME 117, NUMBER 5 MARCH 1, 1960

# Nuclear Shell Effects in $\mu^-$ Capture*

G. H. BURKHARDT†
*Columbia University, New York, New York*

AND

C. A. CAINE
*Clarendon Laboratory, Oxford, England*

(Received September 18, 1959)

The total capture rate for $\mu^-$ mesons in complex nuclei can give some information on the spin-dependence of the weak interaction, by utilizing the variation from one nucleus to another of the spin-dependence of the nuclear transition. The calculation was carried out for $N^{14}$, $O^{16}$, and $F^{19}$, using shell-model wave functions which included configurational mixing in the unfilled shell. The result is not sufficiently spin sensitive to determine the Fermi and Gamow-Teller couplings separately at this stage, but it is in accord with the universal $V$-$A$ hypothesis, if a conserved vector current pion-lepton interaction is included.

## I. INTRODUCTION

WHILE the idea of a universal Fermi interaction, with the same form of coupling between many pairs of fermions, is not new,[1,2] the progress made in the past few years in the elucidation of the $\beta$-decay interaction and the unifying ideas of Gell-Mann and Feyman and others[3,4] have led to a fairly well-defined form, which can be tested for other processes. It has been remarked[3] that the present information on $\mu$ decay fits this form with considerable precision, though it does not, of course, determine it uniquely.

The $\mu$-capture process is the one most closely analogous to $\beta$ decay and it is therefore of interest to find what we can about the interaction Hamiltonian. Because of the $Z^4$ dependence of the capture rate,[5] the experiments on hydrogen, which would give the clearest answers, are not yet possible, so we must learn what we can from the results available. These are principally just the total capture rates which have been measured for a large number of elements with $Z>4$.[6–8] Recently some measurements have also been made on $C^{12}$ of the capture rate to a particular final state.[9]

The total capture rate reflects principally the average coupling constant and an accurate value for this is one objective of such experiments. However, because the spin-dependence of the selection rules for the nuclear transition varies from nucleus to nucleus, mainly due to Pauli exclusion effects, we may learn something about the form of the interaction. This possibility was explored in a calculation by Tolhoek and Luyten,[10] who found, on the basis of a simple shell-model picture of the nucleus, that these shell selection rules produced variations of up to 50% in the nuclear transition probabilities. Their results are, as they say, of semi-quantitative significance only. It is our object to see what modifications can be made to improve on their approximations, and what limits can be placed on the coupling constants.

* Supported in part by the U. S. Atomic Energy Commission and the United Kingdom Department of Scientific and Industrial Research.

† Now at California Institute of Technology, Pasadena, California.

[1] G. Puppi, Nuovo cimento **5**, 587 (1948).

[2] J. Tiomno and J. A. Wheeler, Revs. Modern Phys. **21**, 153 (1949).

[3] R. P. Feynman and M. Gell-Mann, Phys. Rev. **109**, 193 (1958).

[4] S. S. Gershtein and Ya. B. Zeldovich, Zhur. Exptl. i Teoret. Fiz. U. S. S. R. **29**, 698 (1955) [translation: Soviet Phys.-JETP **2**, 576 (1956)].

[5] J. A. Wheeler, Revs. Modern Phys. **21**, 133 (1949).

[6] Sens, Swanson, Telegdi, and Yovanovitch, Phys. Rev. **107**, 1464 (1957).

[7] Astbury, Kemp, Lipman, Muirhead, Voss, Zangger, and Kirk, Proc. Phys. Soc. (London) **72**, 494 (1958).

[8] J. Sens, Phys. Rev. **113**, 679 (1959); and University of Chicago Ph.D. thesis (unpublished).

[9] See A. Fujii and H. Primakoff, Nuovo cimento **12**, 327 (1959).

[10] H. A Tolhoek and J. Luyten, Nuclear Phys. **3**, 679 (1957).